Electronic Supplementary Information (ESI)

Environmental-adaptive quasi-solid-state zinc-ion battery based on magnesium vanadate hydrate with commercial-level mass loading and anti-freezing gel electrolyte

Weijun Zhou,[a] Jizhang Chen,*[a] Minfeng Chen,[a] Anran Wang,[a] Aixiang Huang,[a] Xinwu Xu,[a] Junling Xu*[b] and Ching-Ping Wong[bc]

[a] *College of Materials Science and Engineering, Nanjing Forestry University, Nanjing 210037, China*

[b] *Department of Electronic Engineering, The Chinese University of Hong Kong, NT, Hong Kong, China*

[c] *School of Materials Science and Engineering, Georgia Institute of Technology, Atlanta, United States*

E-mail addresses: chenjizhang@njfu.edu.cn (J. Chen) and junlingxu@outlook.com (J. Xu).

Experimental details

Measurements of ionic conductivity

The ionic conductivity σ of PVA/G gel electrolyte at different temperatures can be estimated by EIS on a VSP-300 electrochemical workstation (Bio-Logic) with an AC amplitude of 5 mV in the frequency ranging from 100 kHz to 0.01 Hz:

$$\sigma = \frac{L}{RS} \qquad (1)$$

where L and S are the thickness and area of the gel electrolyte, and R (Ω) represents the bulk resistance determined from the intercept of Nyquist plots with the real axis.

Supplementary figures

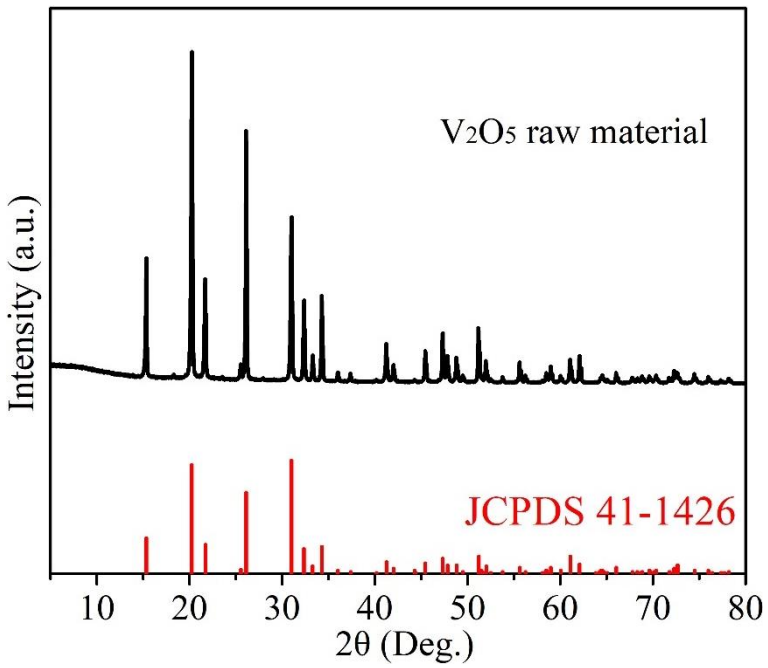

Fig. S1 XRD pattern of V_2O_5 raw material.

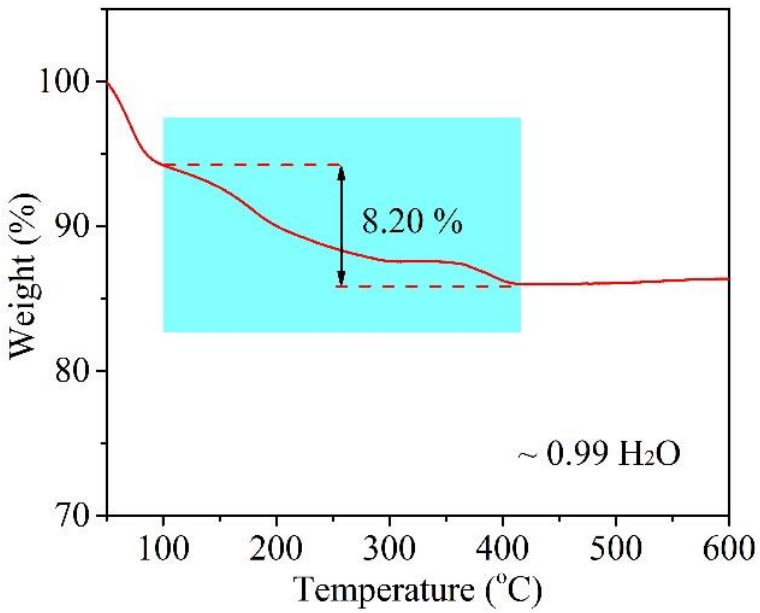

Fig. S2 TGA curve of δ-MgVO in the Ar atmosphere.

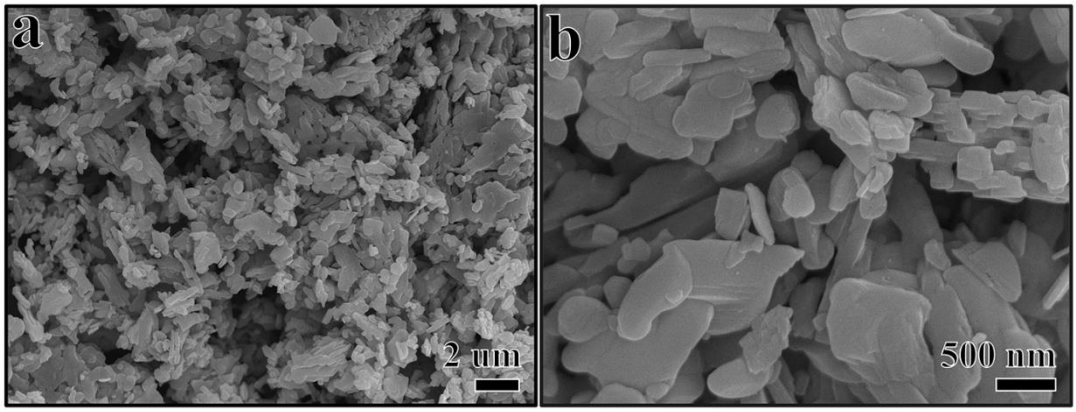

Fig. S3 (a, b) SEM images of V_2O_5 raw material.

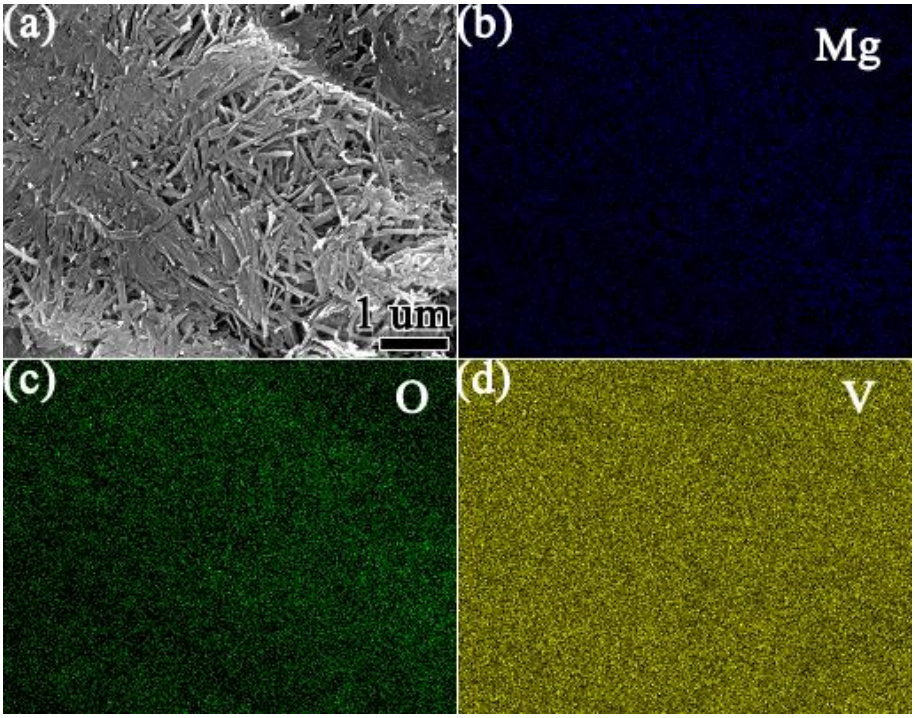

Fig. S4 SEM-EDX mapping images of δ-MgVO.

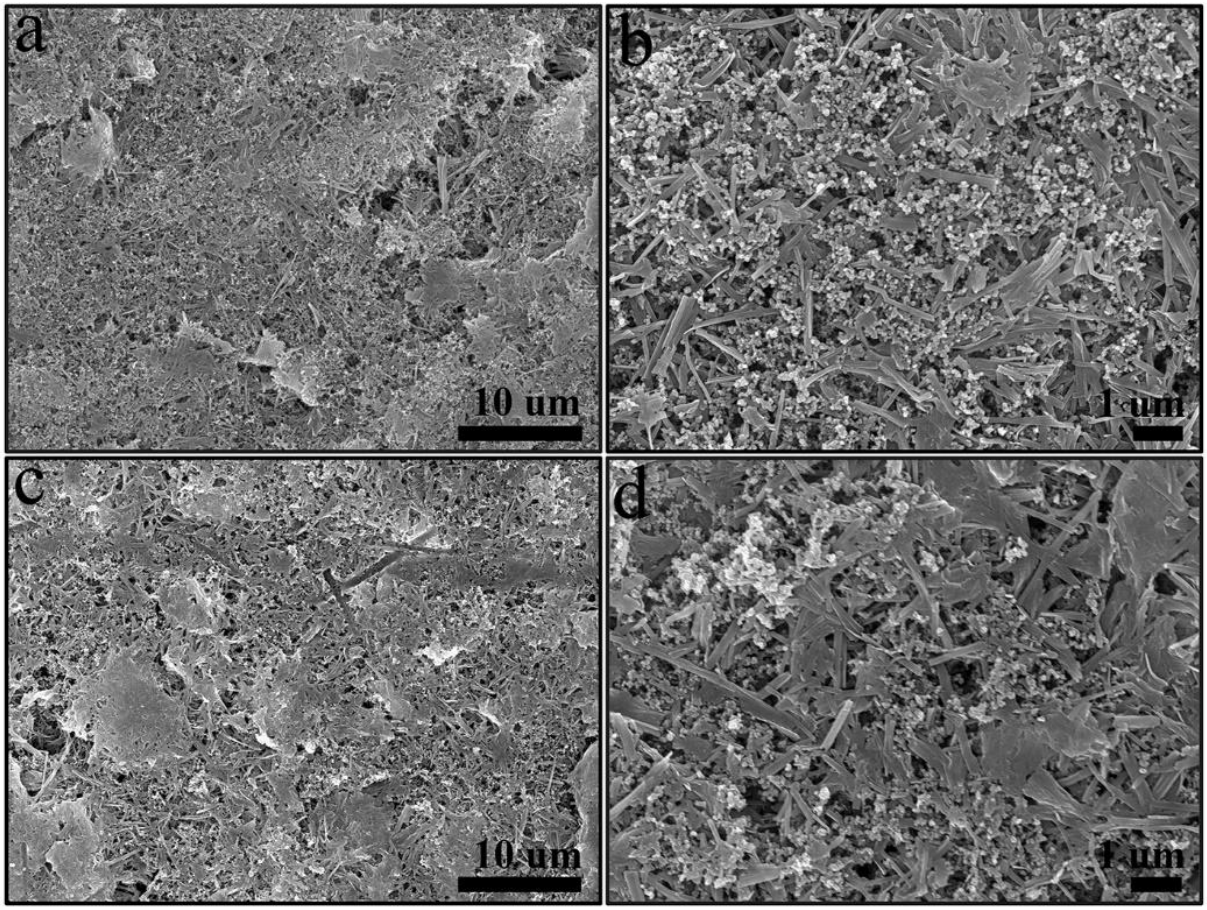

Fig. S5 SEM images of δ-MgVO electrodes: (a, b) before cycles and (c, d) after 5,000 cycles.

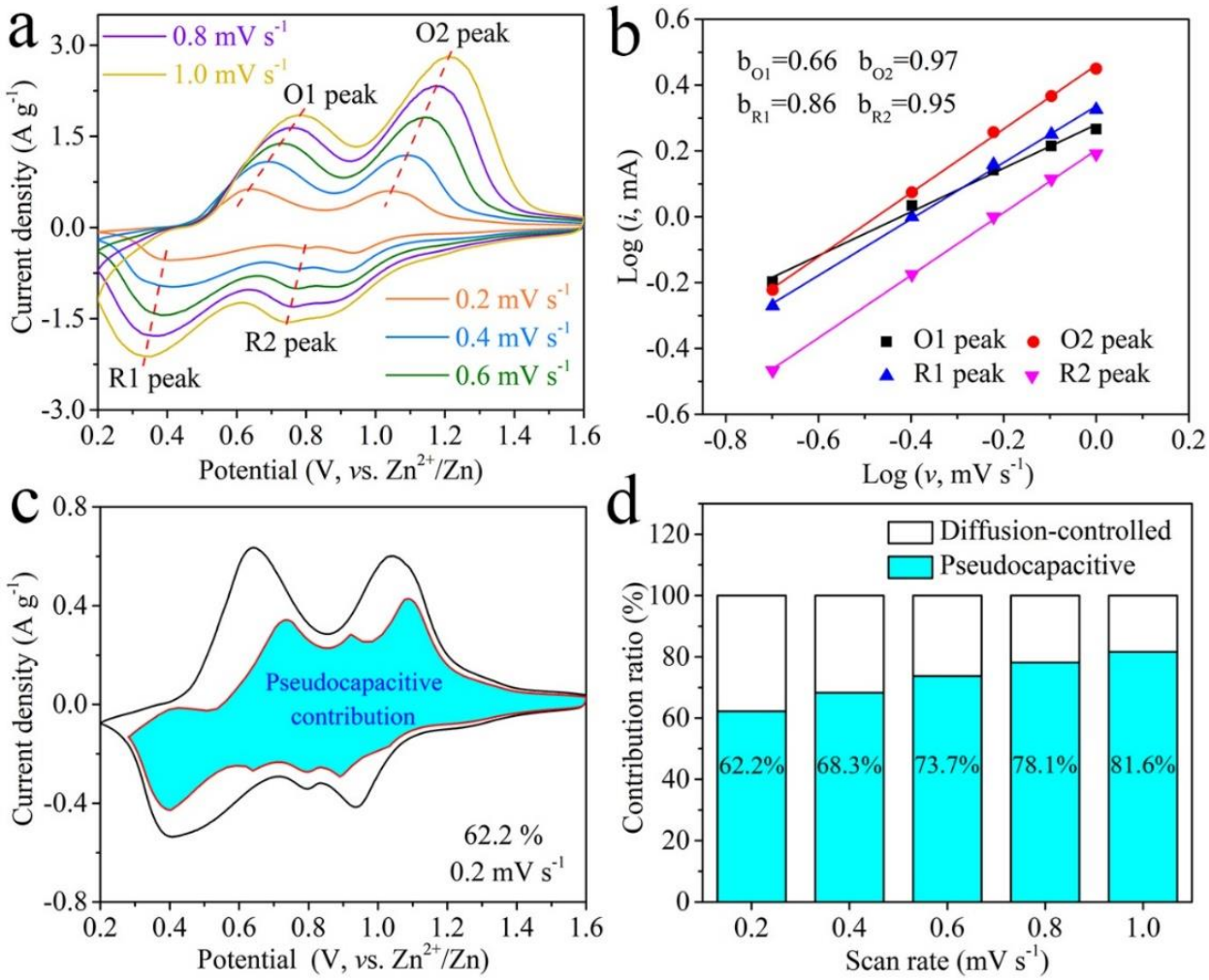

Fig. S6 (a) CV curves of δ-MgVO at scan rates from 0.2 to 1.0 mV s^{-1}. (b) log (*i*) vs. log (*v*) for different redox peaks in the CV curves. (c) capacity contribution analysis of δ-MgVO at 0.2 mV s^{-1}. (d) contribution ratios of diffusion-controlled and pseudocapacitive capacities of δ-MgVO at each scan rate.

Fig. S6a shows CV profiles of δ-MgVO at scan rates from 0.2 to 1.0 mV s^{-1}. These profiles display two couples of redox peaks, whose shapes are similar with increasing the scan rate. The general relationship between the peak current (*i*) and scan rate (*v*) can be described using the following equation if assuming that *i* obeys a power-law relationship with *v*:[1]

$$i = av^b \qquad (2)$$

Generally, the b value of 0.5 and 1.0 represents diffusion-controlled and pseudocapacitive charge storage, respectively. The b values associated with four redox peaks of δ-MgVO are fitted to be 0.66, 0.97, 0.86, and 0.95 (Fig. S6b), indicating the charge storage of δ-MgVO is dominated by the

pseudocapacitive intercalation of electrolyte ions.[2-4] Furthermore, the current response $i(V)$, can be quantitatively divided into capacitive (k_1v) and diffusion-controlled ($k_2v^{1/2}$) parts using the following equation:

$$i(V) = k_1v + k_2v^{1/2} \qquad (3)$$

By determining k_1, it is possible to calculate the fraction of current that arises from pseudocapacitive intercalation as a function of the potential. For instance, in Fig. S6c, at a scan rate of 0.2 mV s^{-1}, the shaded area represents the pseudocapacitive contribution, illustrating that the capacitor-like charge storage behavior in δ-MgVO occurs up to 62.2%. Fig. S6d displays the diffusion-controlled and capacitive contributions to the $i(V)$ at various scan rates. The capacitive contribution ratio increases from 62.2% to 81.6% with the scan rate increasing from 0.2 to 1.0 mV s^{-1}, confirming that the redox process of δ-MgVO is dominated by the pseudocapacitive intercalation, which contributes to great rate capability of δ-MgVO reflected in Fig. 2a.

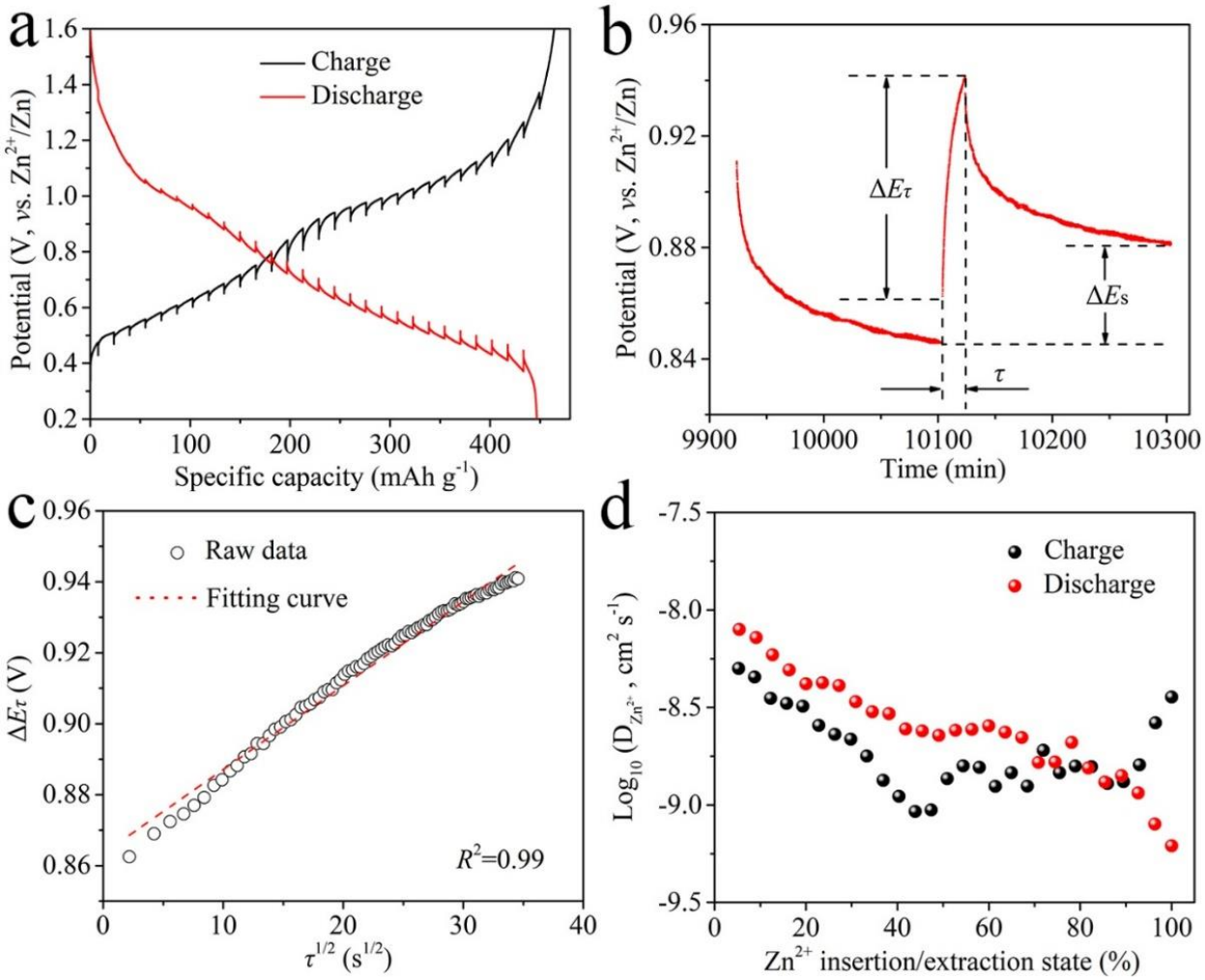

Fig. S7 GITT measurement results of δ-MgVO: (a) charge/discharge curves, (b) schematic illustration of a selected single step of the GITT curve during charging, (c) the linear relationship between ΔE_τ and $\tau^{1/2}$, and (d) the corresponding Zn^{2+} diffusion coefficients.

During the GITT measurement, a current pulse (50 mA g^{-1}) of 1,200 s followed by 3 h relaxation was applied repeatedly (Fig. S7a). The D_{Zn}^{2+} of δ-MgVO could be calculated according to the following equation since ΔE_τ has a linear relationship with $\tau^{1/2}$ (Fig. S7b,c):

$$D_{Zn^{2+}} = \frac{4}{\pi\tau}\left(\frac{n_M V_M}{S}\right)^2\left(\frac{\Delta E_s}{\Delta E_\tau}\right)^2 \qquad (4)$$

where τ is the constant current pulse duration (1,200 s); n_M and V_M are the moles and molar volume of δ-MgVO, respectively; S is the geometric area of δ-MgVO electrode; and ΔE_s and ΔE_τ are the change in the steady state voltage and the overall cell voltage regardless of the *IR*-drop during a single GITT pulse, respectively. The calculated D_{Zn}^{2+} values of δ-MgVO at different states are plotted in Fig. S7d.

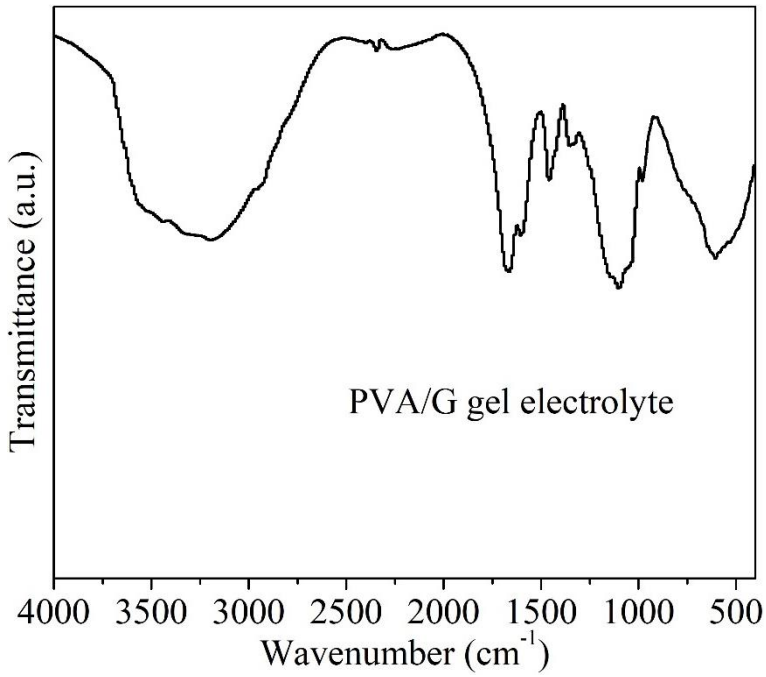

Fig. S8 FTIR spectrum of the dried PVA/G gel electrolyte.

The bands at around 3233, 1656, 1441, 1337, 1100, and 589 cm^{-1} are ascribed to the O–H stretching, O–H bending, symmetric CH_2 bending, CH_2 wagging, C–O stretching, and C–C stretching, respectively.

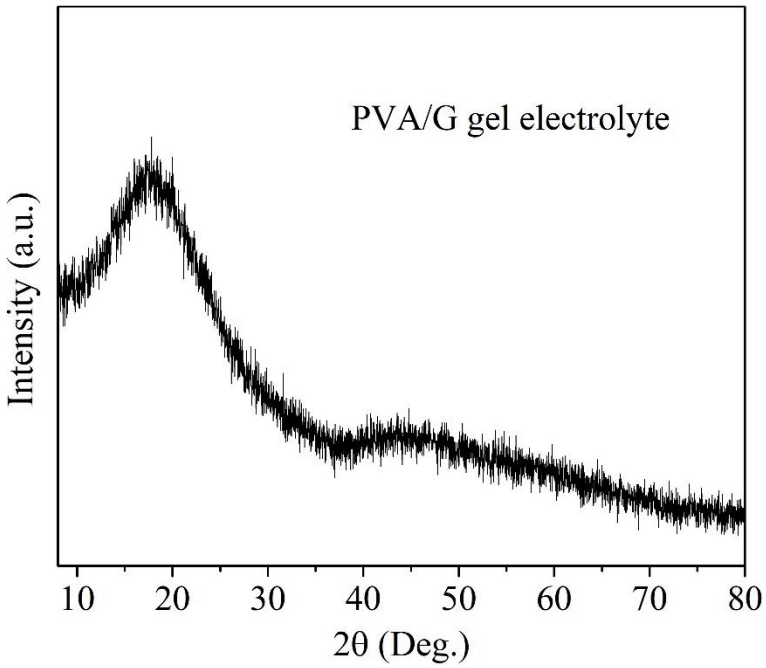

Fig. S9 XRD pattern of the dried PVA/G gel electrolyte.

The broad peak centered at around 18.1^{o} is assigned to the (101) semi-crystalline plane of PVA.

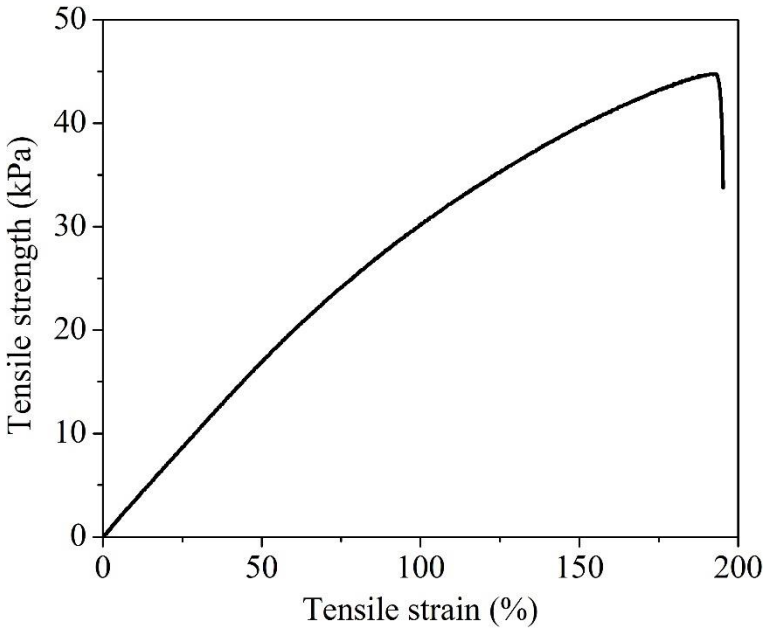

Fig. S10 Tensile σ-ε curve of PVA/G gel electrolyte.

Table S1. The ionic conductivity comparison of PVA/G gel electrolyte in this work with recently reported gel electrolytes for AZIBs. Unless specified, the ionic conductivity values from the literature were obtained at R.T..

Gel electrolyte	Ionic conductivity (mS cm^{-1})	Ref.
PVA/G	18.2 at 25 °C 14.3 at 0 °C 10.7 at –30 °C	This work
PVA	12.6	[5]
PVA-COOH	25.8	[6]
EG-waPUA/PAM	16.8 at 25 °C 14.6 at –20 °C	[7]
PAM	9.1 at 25 °C 1.5 at –15 °C	[8]
Xanthan gum	16.5 at R.T. 2.5 at –8 °C	[9]
HPE	17.6 at R.T.	[10]
Fumed silica	8.1	[11]
PEO	2-4	[12]
PEO/PPO	6.33	[13]
Guar gum	10.7	[14]
Gelatin	6.1	[15]
PVDF-HFP	3.8	[16]

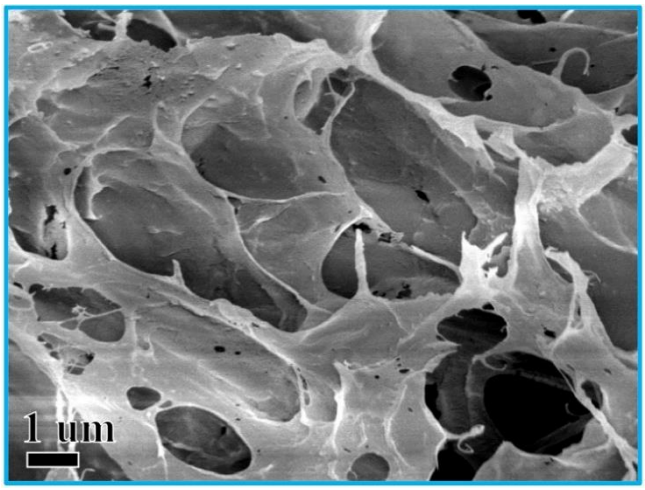

Fig. S11 SEM image of the freeze-dried PVA/G gel electrolyte.

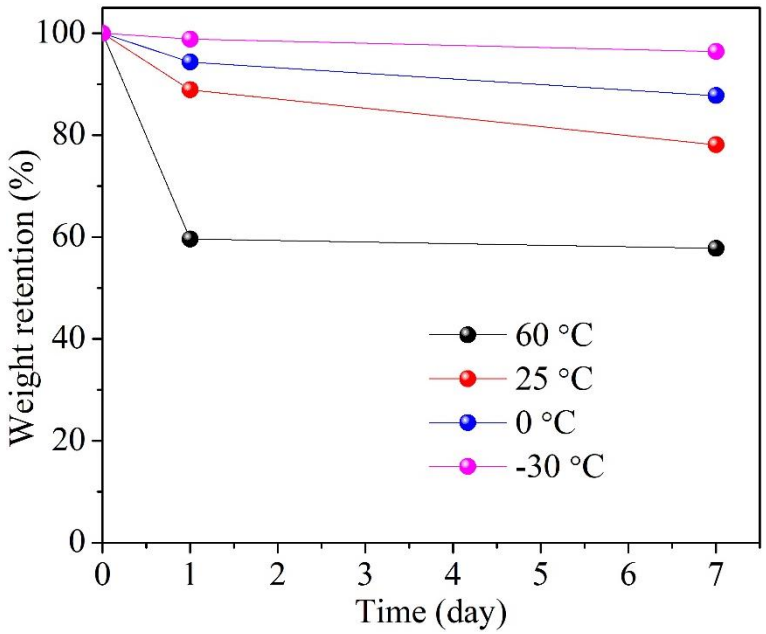

Fig. S12 The weight retention of PVA/G gel electrolyte in the air atmosphere at different temperatures.

Fig. S13 Photograph of measuring the thickness of a thin-film PVA/G Zn//δ-MgVO battery with a micrometer caliper.

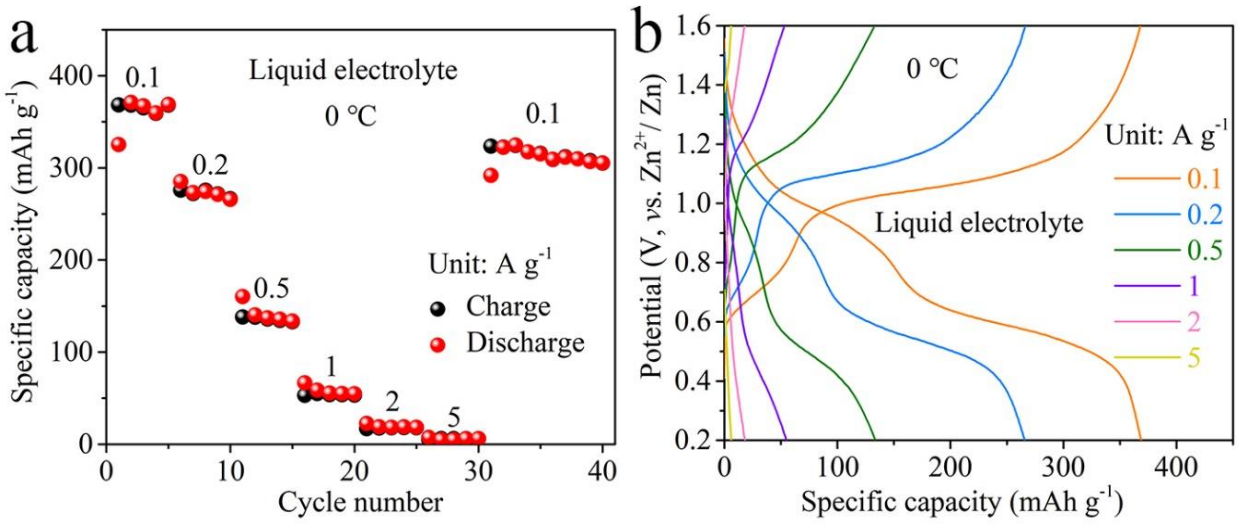

Fig. S14 (a) Rate performance of δ-MgVO in 1 M $Zn(CF_3SO_3)_2$ liquid electrolyte at current densities from 0.1 to 5 A g^{-1} at 0 °C and (b) the corresponding GCD curves.

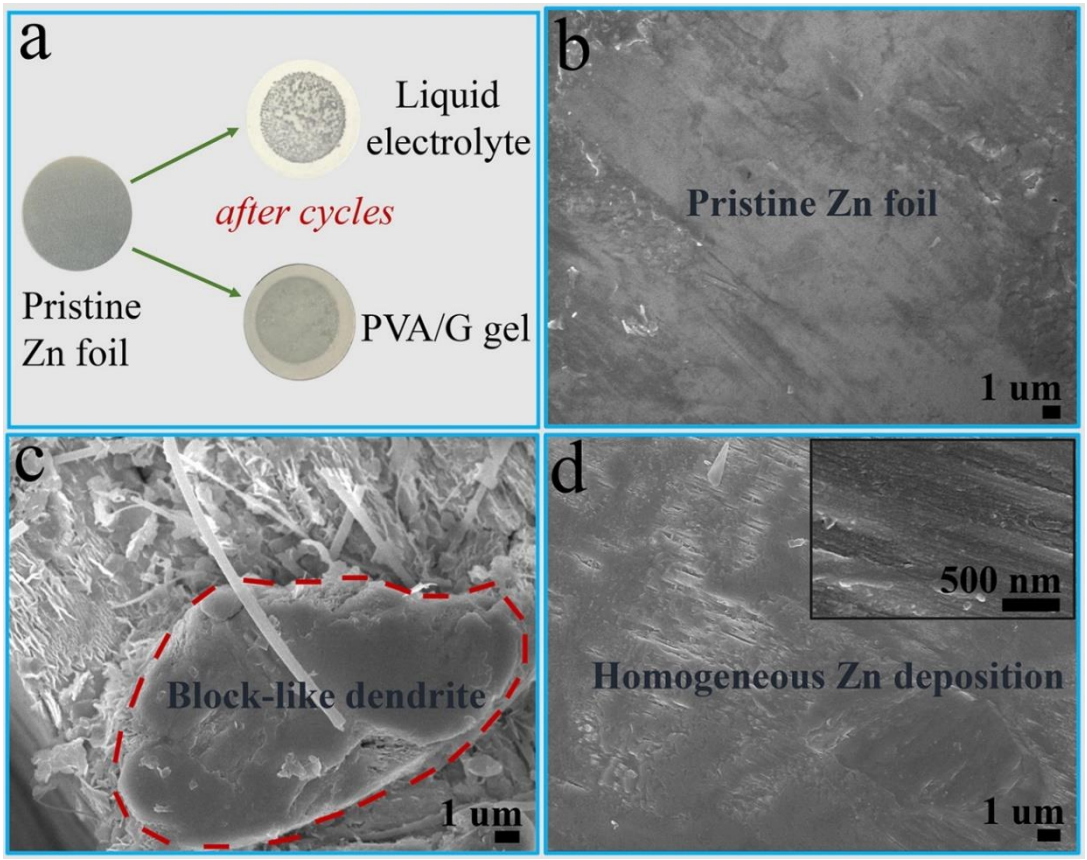

Fig. S15 (a) Photographs of Zn foils at pristine state, with liquid electrolyte after 5,000 cycles, and with PVA/G gel electrolyte after 5,000 cycles. SEM images of (b) pristine Zn foil, (c) Zn foil with liquid electrolyte after 5,000 cycles, and (d) Zn foil with PVA/G gel electrolyte after 5,000 cycles.

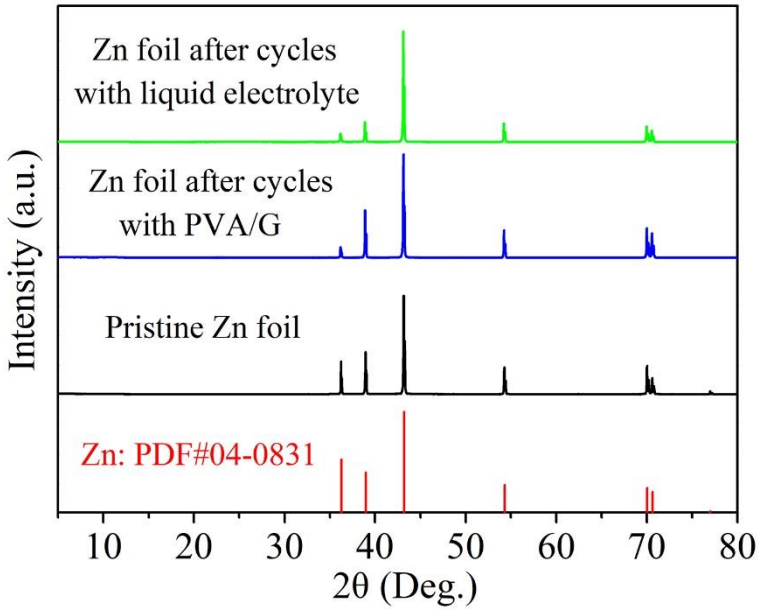

Fig. S16 XRD patterns of the Zn foils at pristine state and after 5,000 cycles with different electrolytes.

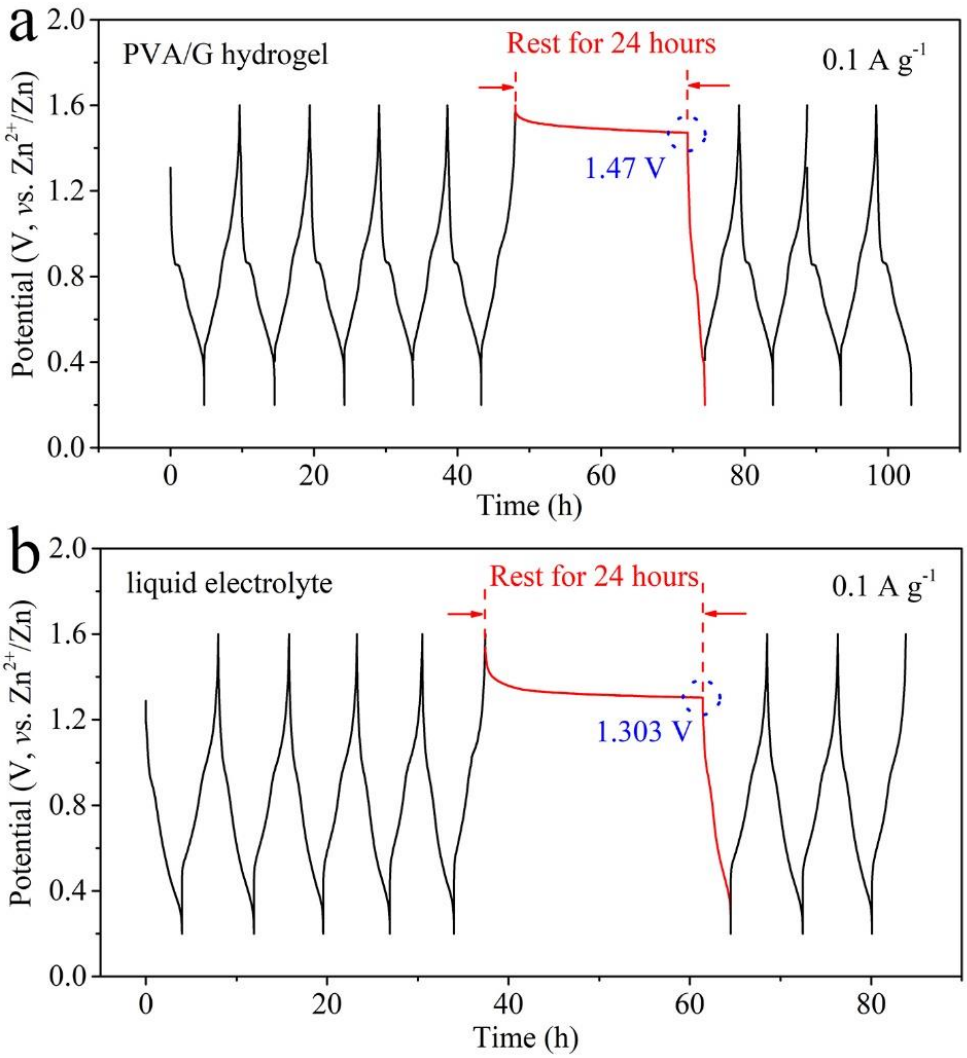

Fig. S17 Self-discharge tests of Zn//δ-MgVO batteries: (a) with PVA-G gel electrolyte and (b) with liquid electrolyte.

The batteries were charged/discharged for five cycles at 0.1 A g^{-1}, followed by 24 h rest, and then continued to be cycled at the same current density. The open-circuit potential (OCP) of PVA/G battery and liquid-electrolyte battery drops to 1.470 and 1.303 V after the 24 h rest, respectively, indicative of slow self-discharge behavior. What's more, the PVA/G battery shows slower self-discharge behavior than the liquid-electrolyte battery. And the lost capacity is recoverable in the subsequent cycles. These results further confirm high reliability of our PVA/G battery.

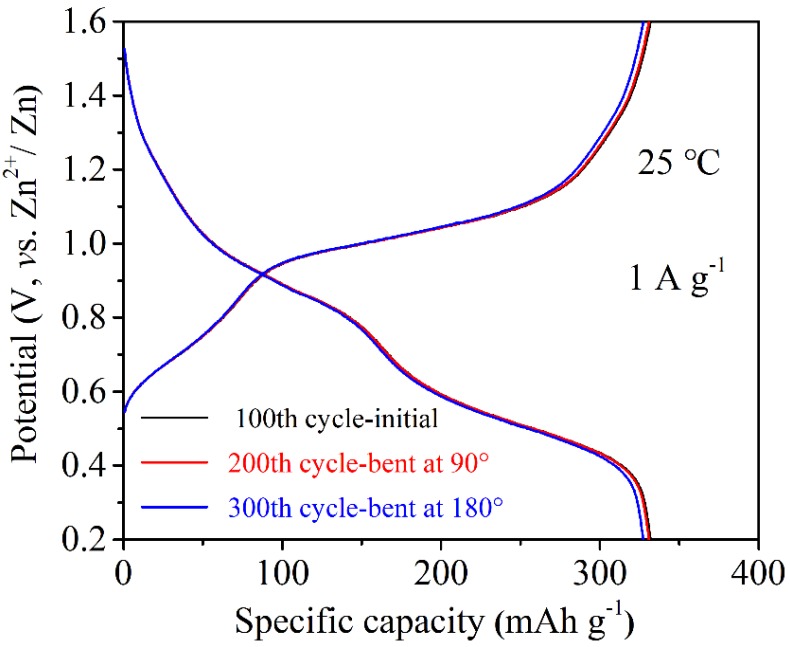

Fig. S18 GCD curves of the thin-film PVA/G Zn//δ-MgVO battery at different bending angles (corresponding to the cycling-performance test in Fig. 6a).

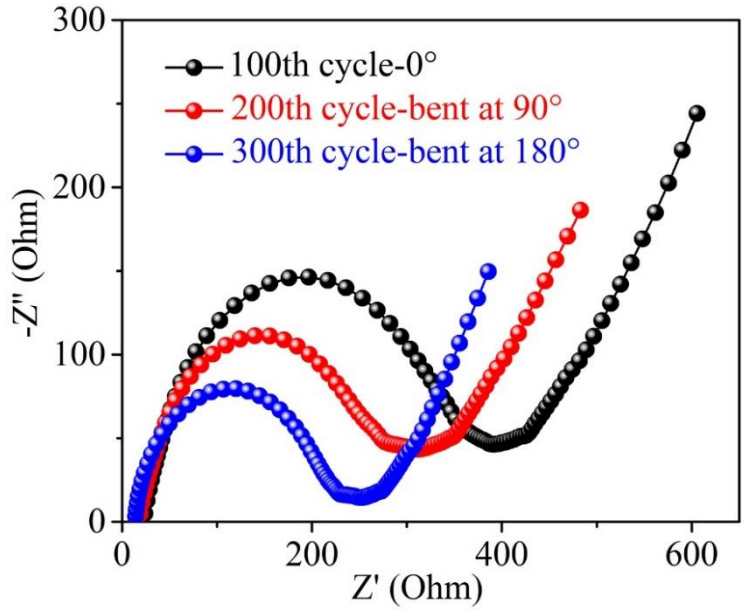

Fig. S19 Nyquist plots of the thin-film PVA/G Zn//δ-MgVO battery after 100th, 200th, and 300th cycles at different bending angles (corresponding to the cycling-performance test in Fig. 6a).

Supplementary videos

Video S1 Demonstration of a thin-film PVA/G Zn//δ-MgVO battery powering an electric fan under repeated bending.

Video S2 Demonstration of a PVA/G Zn//δ-MgVO battery sealed in solid ice (taken out from a –30 °C high-low temperature chamber) powering an electric timer.

References

1 V. Augustyn, J. Come, M. A. Lowe, J. W. Kim, P. L. Taberna, S. H. Tolbert, H. D. Abruna, P. Simon and B. Dunn, *Nat. Mater.*, 2013, **12**, 518-522..

2 D. Kundu, B. D. Adams, V. Duffort, S. H. Vajargah and L. F. Nazar, *Nat. Energy*, 2016, **1**, 16119.

3 F. Ming, H. Liang, Y. Lei, S. Kandambeth, M. Eddaoudi and H. N. Alshareef, *ACS Energy Lett.*, 2018, **3**, 2602-2609.

4 Y. Liu, C. Li, J. Xu, M. Ou, C. Fang, S. Sun, Y. Qiu, J. Peng, G. Lu, Q. Li, J. Han and Y. Huang, *Nano Energy*, 2020, **67**, 104211.

5 S. Huang, F. Wan, S. Bi, J. Zhu, Z. Niu and J. Chen, *Angew. Chem. Int. Edit.*, 2019, **58**, 4313-4317.

6 Q. Li, X. Cui and Q. Pan, *ACS Appl. Mater. Interf.*, 2019, **11**, 38762-38770.

7 F. Mo, G. Liang, Q. Meng, Z. Liu, H. Li, J. Fan and C. Zhi, *Energy Environ. Sci.*, 2019, **12**, 706-715.

8 X. Li, L. Ma, Y. Zhao, Q. Yang, D. Wang, Z. Huang, G. Liang, F. Mo, Z. Liu and C. Zhi, *Mater. Today Energy*, 2019, **14**, 100361.

9 X. Cheng, L. Zhou, Y. Lu, W. Xu, P. Zhang and X. Lu, *Electrochim. Acta*, 2018, **263**, 311-317.

10 H. Li, C. Han, Y. Huang, Y. Huang, M. Zhu, Z. Pei, Q. Xue, Z. Wang, Z. Liu, Z. Tang, Y. Wang, F. Kang, B. Li and C. Zhi, *Energy Environ. Sci.*, 2018, **11**, 941-951.

11 D. Chao, C. R. Zhu, M. Song, P. Liang, X. Zhang, N. H. Tiep, H. Zhao, J. Wang, R. Wang, H. Zhang and H. J. Fan, *Adv. Mater.*, 2018, **30**, 1803181.

12 A. Turković, M. Pavlović, P. Dubček, M. Lučić-Lavčević, B. Etlinger and S. Bernstorff, *J. Electrochem. Soc.*, 2007, **154**, 554-560.

13 J. Zhao, K. K. Sonigara, J. Li, J. Zhang, B. Chen, J. Zhang, S. S. Soni, X. Zhou, G. Cui and L. Chen, *Angew. Chem. Int. Edit.*, 2017, **56**, 7871-7875.

14 Y. Huang, J. Zhang, J. Liu, Z. Li, S. Jin, Z. Li, S. Zhang, H. Zhou, *Mater. Today Energy*, 2019, **14**, 100349..

15 Q. Han, X. Chi, S. Zhang, Y. Liu, B. Zhou, J. Yang and Y. Liu, *J. Mater. Chem. A*, 2018, **6**, 23046-23054.

16 J. P. T. Guisao and A. J. F. Romero, *Electrochim. Acta*, 2015, **176**, 1447-1453.